

Article

A Molecular Understanding of the Flame Retardant Mechanism of Zinc Stannate/Polypropylene Composites via ReaxFF Simulations

Jun Li ¹, Meilin Zhu ², Chang Geng ^{3,*}, Yingjie Yuan ¹, Zewei Fu ¹, Shu Yan ³, Rou Feng ³, Yingwu Wang ⁴, Ying Zhou ⁴, Liangliang Meng ³, Hui Zhang ³ and Hongcun Bai ^{3,*}¹ Yunnan Tin Industry Group (Holding) Co., Ltd., R & D Center, Kunming 650200, China² College of Basic Medical Sciences, Ningxia Medical University, Yinchuan 750004, China³ State Key Laboratory of High-Efficiency Utilization of Coal and Green Chemical Engineering, College of Chemistry and Chemical Engineering, Ningxia University, Yinchuan 750021, China⁴ Yunnan Provincial Academy of Science and Technology, No. 488 Dianchi Road, Kunming 650051, China

* Correspondence: gengchang1111@163.com (C.G.); hongcunbai@nxu.edu.cn (H.B.)

Abstract: As an important new flame retardant, zinc stannate (ZS) shows wide application prospects due to its many advantages. However, the flame retardant mechanism of composites made with polymer combined with ZS is still unclear. In particular, there is a lack of molecular level description of the micro-scale flame retardant mechanism. The combustion mechanism through molecular simulation technology has become an important research paradigm in the field of fire, which can provide new insights for the development of new materials. This work studied the flame retardant mechanism of composites consistent with polypropylene (PP) and ZS using reactive force field molecular dynamics (ReaxFF MD) simulations. A new force field incorporating Sn/Zn/C/H/O components for ZS/PP composites combustion reactions was developed. Twenty different ZS/PP composites were analyzed for their combustion reactions at various temperatures. To investigate the flame retarding mechanism of ZS in composites, the evolutions of reactants, products, and reaction intermediates at the molecular scale were collected. It was revealed that the combustion temperature controlled the degree of oxidation by regulating the consumption of molecular oxygen during PP cracking. An increased combustion temperature reduced the oxygen consumption rate and overall oxygen consumption. As the PP component of composites exceeded 56%, oxygen consumption increased. Evolutions for carbon-containing intermediates and the products in combustions of PP/ZS composites were analyzed. The small carbon-based fragments were more likely to be produced for composites with low PP contents at high temperatures. These results are beneficial to design ZS/PP composites as flame retardant materials.

Keywords: flame retardant; zinc stannate; polypropylene; ReaxFF MD; combustion

Citation: Li, J.; Zhu, M.; Geng, C.; Yuan, Y.; Fu, Z.; Yan, S.; Feng, R.; Wang, Y.; Zhou, Y.; Meng, L.; et al. A Molecular Understanding of the Flame Retardant Mechanism of Zinc Stannate/Polypropylene Composites via ReaxFF Simulations. *Inorganics* **2023**, *11*, 233. <https://doi.org/10.3390/inorganics11060233>

Academic Editor: Roberto Nisticò

Received: 17 March 2023

Revised: 10 May 2023

Accepted: 18 May 2023

Published: 27 May 2023



Copyright: © 2023 by the authors. Licensee MDPI, Basel, Switzerland. This article is an open access article distributed under the terms and conditions of the Creative Commons Attribution (CC BY) license (<https://creativecommons.org/licenses/by/4.0/>).

1. Introduction

As one of the most popular plastics in the world, polypropylene (PP) has attracted wide attention due to many advantages, such as its low price, excellent mechanical properties, heat resistance, corrosion resistance, and easy processing [1–4]. It is utilized in many industrial production and human life domains [5,6]. One of the disadvantages of polypropylene is that it is flammable, and the limiting oxygen index (LOI) is only approximately 17.4% [7,8]. Many heat and molten droplets can rapidly spread the flame during combustion and generate an inferno. In addition, smoke and dripping accompany the sound. Thus, PP in the combustion process will produce a large amount of toxic smoke and other corrosive gases, including CO/HCN and other choking gases, as well as HCl/HBr/NO_x/SO_x and other irritating gases [9]. These toxic agents can quickly suffocate people, severely hampering firefighting efforts and evacuations [10]. This method severely

restricts the field of PP application [11,12]. Hence, PP-based goods must undergo flame-retardant modification to fulfill application requirements. Thus, flame retardant and smoke suppression of PP-based materials are of enormous practical importance for ensuring the safety of people's lives and property. Research on the flame retardancy of PP has become a significant concern [13].

There have been reports of studies on the flame-retardant properties of PP. Antimony trioxide (Sb_2O_3), copper oxide (CuO), zinc oxide (ZnO), and molybdenum trioxide (MoO_3) have been used as flame retardants for PP materials [14,15]. Standard flame retardant systems contain significant levels of bromine and antimony, which are detrimental to human and environmental health. Alternatively, the large filling volume and poor compatibility with PP drastically decrease the appearance and qualities of the matrix resin and the end product [16].

Among many flame retardants, zinc stannate (ZS) is a highly efficient inorganic additive flame retardant [17]. ZS is a semiconducting oxide compound consisting of three components [18]. Compared with binary oxides, ternary oxides such as ZS are chemically more stable, making them ideal for applications in extreme conditions; for example, ZS was used in flame retardants and smoke inhibitors. As an inverse spinel structure, ZS is a promising n-type ternary semiconductor that has a wide band gap of 3.6 eV (space group $\text{Fd}\bar{3}m$) [19]. So, in addition to playing an important role in advanced technologies such as gas sensors, photocatalytic materials, and zinc-tin-oxide transistors, ZS also has a presence in the field of co-flame retardants.

ZS, as a premium flame retardant substitute for antimony trioxide, is preferred due to its effective flame retardant and smoke suppression properties, as well as the fact that it is non-toxic and safe [20,21]. ZS can be used alone or with other flame retardants [22,23]. ZS has drawbacks, including expensive and restricted resources, aggregation in the polymer matrix, low dispensability, and compatibility. High-performance molecular dynamics calculations can be used to study the similarities and differences of the micro-combustion process of plastics with different components and contents in the presence of tin-based flame retardants, which can provide a theoretical basis for the optimization of composite formulation design.

Fire is mostly a process of intense combustion caused by chemical reactions. The reaction mechanism of the combustion process, such as reaction path, reaction exothermic property, and products, determines the fire risk. Understanding the detailed reaction mechanism of the combustion process, such as the reaction micro-mechanism and combustion process, is the key to mastering the combustion induction and evolution mechanism in essence, which can provide scientific guidance for the effective prevention and control of fire accidents and also provide a theoretical basis for the development of new flame retardants and fireproof materials [24]. However, the chemical reaction in the combustion process is very complex and thus not easy to explore. There are two main methods used to study the reaction mechanism: experimental means and molecular simulation technology. The experimental method can obtain the characteristics of reactants, intermediates, and main products in the reaction process with the help of various analysis and characterization instruments and then infer and predict the reaction mechanism. For example, in situ, infrared spectroscopy, online mass spectrometry, and other major characterization methods can be used, supplemented by thermal analysis methods such as temperature-programmed and differential scanning calorimetry, to study the change rules of chemical reactions [25]. These can undoubtedly provide the change characteristics of free radicals and functional groups in the oxidation process of combustible materials and speculate on the oxidation reaction mechanism of typical functional groups.

Although advanced experimental analysis and characterization methods can obtain the characteristics of some intermediates, including products and free radicals, in the reaction process and reasonably speculate on the reaction mechanism [26], however, there is still a lack of effective experimental detection means for radical, intermediate, and complex microscopic reaction paths that change rapidly under more severe combustion

conditions [27]. On the other hand, the combustion and pyrolysis of polymers are driven by free radicals and involve many coupled reaction pathways [28]. It is noticed that capturing free radical fragments with high activity and short lifetimes is difficult using only experimental techniques. The intermediates in combustion products can influence the transformation of the product structure [29]. Tracing the detailed evolutionary process of their involvement in the reaction using experimental techniques is complicated and expensive. This could limit deep exploration of the complex flame retardant reaction processes and the generation pathways of products. Therefore, understanding the essence of flame retardant at the atomic level is not an easy task. It is very difficult to understand the mechanism of explosion reactions only by experimental means. This undoubtedly prompted researchers to turn their attention to computer molecular simulation methods. With the help of rapidly developing computer technology, scholars expect to obtain the detailed microscopic reaction mechanism of the chemical explosion process at the theoretical and molecular levels [30].

Nowadays, molecular simulations have become more and more crucial in the studies of materials science, in particular for mechanism analysis [31]. It can give more insights into tracing the detailed evolutionary process in the reaction beyond the experiments. Thus computational chemical simulation provides essential advantages for exploring the dynamic evolution of the flame retardancy of inorganic materials [32]. It has become an indispensable tool for supplementing experimental observations. ZS applied to PP flame retardant products has a good flame retardant and smoke suppression effect. In this work, we adopted a ReaxFF MD simulation, providing insights into flame retardant performance and mechanism for ZS/PP composites.

In this study, the flame retardant mechanism of ZS/PP composites was studied using reactive force field molecular dynamics (ReaxFF MD) simulations. In order to perform the ReaxFF calculations, a force field containing Sn/Zn/C/H/O elements for the combustion reactions of ZS/PP composites was developed. The molecular quantity changes of reactants, products, and primary reaction intermediate during the combustion of 20 different ZS/PP composites with different contents were investigated at various temperatures. This work could provide theoretical guidance for the design and optimization of ZS/PP composites as flame retardant materials.

2. Results and Discussion

2.1. ReaxFF Force Field Results and Verification

The ground state structure (such as multiple molecular structures in Figure 1) is provided for verification by identifying, constructing, and optimizing specific systems. It is strictly described by quantum chemistry (QM). Finally, by limiting the calculation times to DFT/ReaxFF, the bond length or the selected angle is limited to the range below and above the equilibrium value. The dissociation curve is constructed for the structure. The ability of metal atoms to achieve a high coordination state is related to the strong differentiation of catalysts, so it is essential to characterize the ability of metals to bind multiple carbon groups alone. For Zn and Sn metals, the singlet is built by adding carbon groups to determine the lowest energy spin state of the system, as shown in Figure 1a–d, which facilitates more accurate energy determination and reduces the cost of calculation. Figure 1 represents the interaction energy between different groups and metal atoms, which compares the bond length and bond angle energy difference calculated by the ReaxFF with the energy difference calculated based on the first principle, which is used to proofread and verify the accuracy of the force field. As shown in Figure 1, The C–Sn equilibrium bond lengths calculated by QM are closer to the results of Bernt et al. (2.108–2.146 Å) [33]. On the QM energy spectrum, when the C–Sn bond extends above 3.41 Å, the energy state of the DFT data changes, which ReaxFF well captures by calculating the lowest energy state.

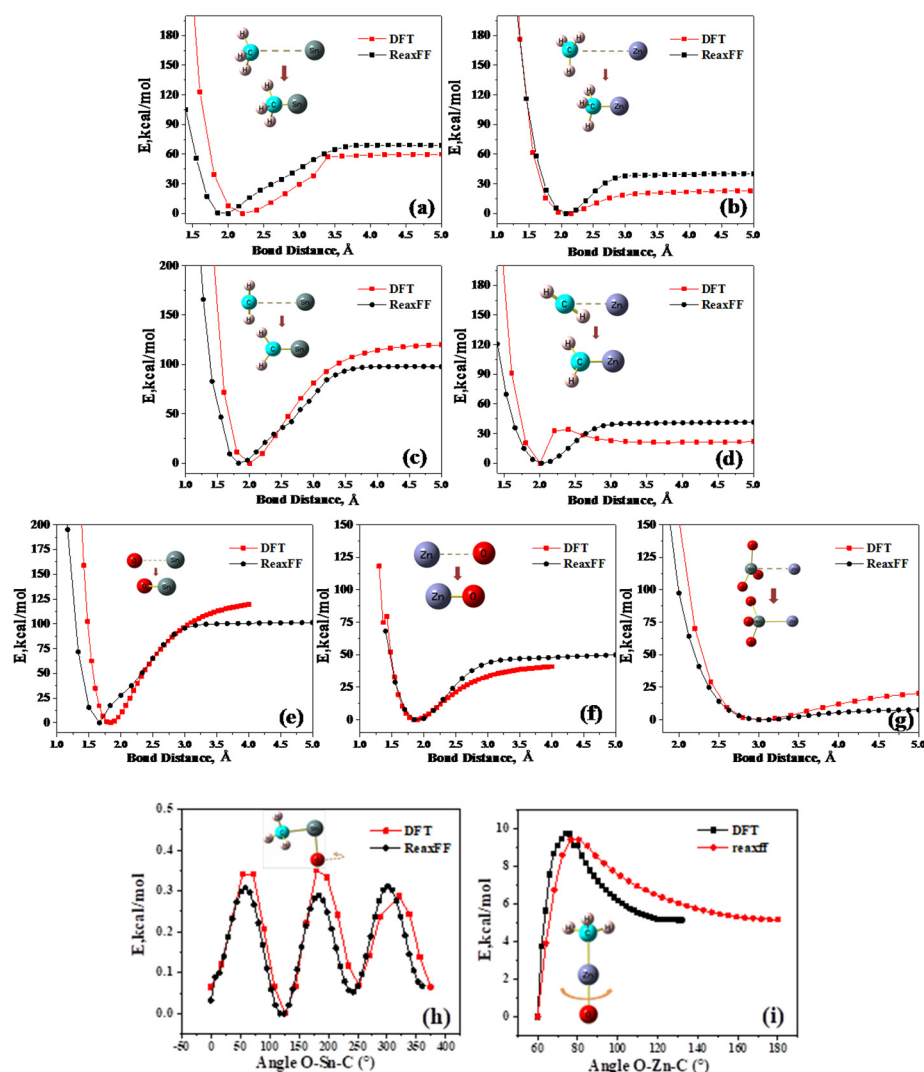


Figure 1. ReaxFF and QM results for bond dissociations and angle distortion in complexes. (a) C–Sn bond in CH_3Sn ; (b) C–Zn bond in CH_3Zn ; (c) C–Sn bond in CH_2Sn ; (d) C–Zn bond in CH_2Zn ; (e) Sn=O bond in SnO; (f) Zn=O bond in ZnO; (g) Sn–Zn bond in ZnSnO_3 ; (h) H–C–Sn–O dihedral angle in CH_3SnO ; and (i) C–Zn–O angle in CH_3ZnO .

In the C–Zn bond dissociation energy of CH_3Zn , the equilibrium bond length predicted by QM and ReaxFF is about 2.07 Å. The error between them is less than 0.05 Å. It is in good agreement with the reported value of Yang et al. [34]. In C–Zn bond stretching, the energy change tends to be stable when the distance between C/Zn atoms in QM and ReaxFF is more significant than 2.953 Å. The set distance of Sn–O bond length DFT is 0.7–4.0 Å, the scanning range of ReaxFF is 1–5 Å, and the equilibrium bond length predicted by QM and ReaxFF is 1.84 and 1.67 Å. The Sn–O equilibrium bond length calculated by QM is closer to the result of Shetty et al. (1.907 Å) [35]. The difference between the ReaxFF dissociation energy of the Sn–O bond and the result of QM is not more significant than that of 25 kcal/mol. The Zn–O bond distance set by DFT is 1.3–4.0 Å, and the scanning range of ReaxFF is 1.4–5.0 Å. The equilibrium bond length of Zn–O predicted by QM and ReaxFF is about 1.9 Å, and the error between them is small, similar to that reported by Wong-Ng et al. (1.91 Å) [36].

The interaction between the Zn and Sn atoms is also considered. Figure 1g shows the bond dissociation curve of $\text{CH}_3\text{Sn–Zn}$. DFT sets the bond distance of Sn–Zn to 1.8–5.8 Å, and the scanning range of ReaxFF is 1.875–5.000 Å. In the scanning distance of 1.875–5.000 Å, the difference between the ReaxFF dissociation energy of the Sn–Zn bond and the QM

result is less than 15 kcal/mol. The Sn–Zn equilibrium bond lengths predicted by QM and ReaxFF are both around 2.8 Å, which is very close to the value of $(\text{Sn}_9\text{ZnR})^{3-}$ compound ($d_{\text{Av}}(\text{Sn}-\text{Zn}) = 2.78 \text{ \AA}$) [37].

In addition to the bond dissociation energy, the degree of freedom of the bond angle bending around the metal is also very important. It shows that new carbon atoms can be coordinated easily [38]. In this section, by constructing the ReaxFF calculation of the oxygen-rich system of ZS, we have obtained some central intermediates and built the structure to provide the most straightforward possible electron arrangement. In this section, to verify the modified force field, the bond dissociation energy in the confirmed object is mainly Me–CH₃/Me=CH₂/Me–O/Me–Me (Figure 1a–g), and the valence torsion energy specifically includes CH₃–Zn–O/CH₃–Sn–O (Figure 1h,i). The verification set of valence angle is selected as the C–Sn–O/C–Zn–O angle in CH₃SnO/CH₃ZnO cluster. Figure 1h is the dihedral angle scan of H–C–Sn–O. As shown in the figure, all the dihedral angles in the DFT calculation are smaller than the rotational barrier of 0.4 kcal/mol, and ReaxFF can reproduce this feature very well. To verify the valence angle parameters of the molecule, we keep a fixed value for each Zn–C–H angle in the CH₃ZnO molecule, and the scanning range of the C–Zn–O angle in QM and ReaxFF is 60–132 and 60–180°, respectively. The DFT and ReaxFF data reached the maximum energy at 74 and 79°, respectively.

It can be seen from the energy correction above that the QM data are in good agreement with the ReaxFF energy changes, and the fitted reaction force field can correctly reflect the potential energy changes of the bond angles of length. Thus, the ReaxFF force field developed here gives good performance in comparison with DFT results.

2.2. Effect of Temperature and Composite on Combustion Reactants

As the ZS flame retardant mechanism is a typical inorganic non-reactive process, providing thermal insulation for polymers by forming a carbon protective layer, and thus plays a role in the condensed phase. This section compares the microscopic combustion phenomena of different formulations of plastics under tin-based flame retardants and the evolution of reactants, intermediates, and products under different temperatures. It provides a theoretical basis for the optimization of composite formula design.

The number statistics of oxygen molecules can more directly observe the flame retardant results and further explain the flame retardant mechanism. Oxygen molecules can promote the degradation of plastic. This idea has been demonstrated in our previous work [39], the polyethylene molecules were attacked by O· free radicals formed by oxygen pyrolysis to occur C–C breaking reaction, and then the polymer was continuously cracked to intermediates with different carbon numbers.

The evolutions of the O₂ number during the PP combustions at different temperatures are shown in Figure 2. It can be seen that the O₂ consumption of combustion systems with various PP percentages is comparable. The higher the combustion temperature, the slower the rate of O₂ consumption, and the smaller the total amount of O₂ used. For 20 PP/ZS composites, O₂ consumption was around 38.5% when the combustion temperature was 1000 K. During the first 10 ps of rapid O₂ consumption, the combustion rate was 1.21 to 1.76 O₂ molecules per picosecond. At 150 ps, the O₂ concentration stabilizes. The O₂ consumption of twenty distinct PP/ZS composites varies as well. When there are thirteen or more PP clusters in PP/ZS composites, the total O₂ consumption increases dramatically and gradually exceeds 50 O₂ molecules.

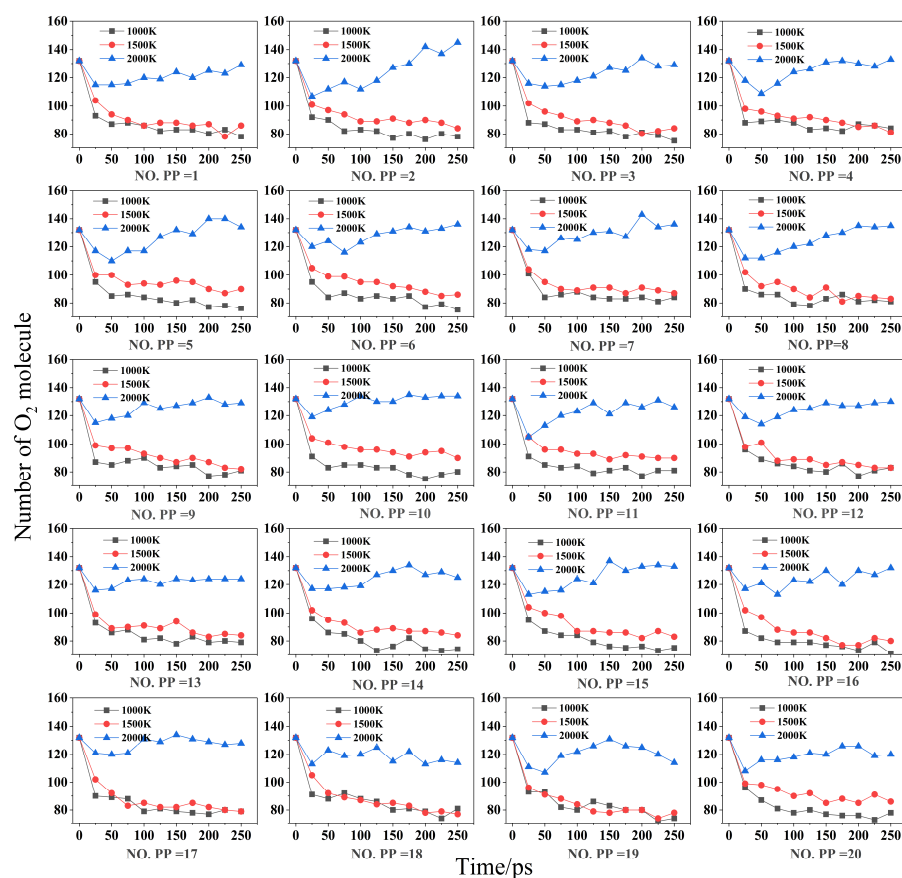


Figure 2. Changes in O_2 molecule number for 20 PP/ZS composites under different combustion temperatures.

When the content of PP in composites was 20–28%, 28–56%, and 80%, O_2 consumption was the lowest in the rapid oxygen consumption stage, and the O_2 consumption rate gradually decreased after 10 ps. When the temperature is 1500 K, the rapid oxygen consumption rate in the first stage is lower than that at 1000 K, and the combustion rate is 1.08–1.20 O_2 per ps. When the PP content in composites is 28/48/76/80%, the rapid oxygen consumption rate in the first stage is the same as the O_2 consumption rate at 1000 K. The number of O_2 is stabilized earlier at 1500 K than at 1000 K. At about 100–150 ps, the proportion of oxygen consumption is relatively low, about 30.8%. When the PP content in composites is 21, 68, and 76%, the total oxygen consumption at 1500K is almost identical to that at 1000 K. With 2000 K for combustion, the oxygen consumption with different PP contents is similar. Within 0–50 ps, the number of O_2 decreases continuously, and the oxygen consumption rate is significantly lower than that under 1000 and 1500 K. About 0.4–0.8 O_2 are consumed per picosecond. Among them, when PP contents are 8/16/20/44/76 and 80%, the oxygen consumption during 0–50 ps at 2000 K is the most, and the O_2 consumed is more than 20. After 50–75 ps, O_2 increased in the system. Through visual analysis, the ZS crystal structure is unstable at 2000 K, which leads to the gradual bond between adjacent oxygen atoms on surfaces. After 1.25 ps, the crystal was detached in the form of $O=O$ and dissociated in the system. At high temperatures, the ZS flame retardant begins with rapid decomposition. Then the number of ZS fragments are fused with PP molecules, hindering the contact between oxygen and PP. After 25 ps, ZS fragments are cross-linked and form the cluster structures near PP, which are dispersed in the system and further hinder the oxidation reaction.

According to Figure 2, 1000 K is the temperature condition with the fastest and maximum oxygen consumption rate. Further analysis was conducted on the number of O_2 with different PP contents at 1000 K, as shown in Figure 3, to study the influence of

PP content on oxygen consumption rate and combustion. As shown in Figure 3a, when polypropylene content is 4–20%, the combustion is the rapid oxygen consumption process in the first stage within 0–25 ps. When the PP content is 12–16%, the oxygen consumption is at its maximum, and the number of O₂ consumed is 44 in the first stage. When the PP content is 4/8/20%, oxygen consumption is less, and the number of O₂ is 38. The second stage is the slow oxygen consumption process after 25 ps. The lowest oxygen consumption was presented in the composites with PP contents of 4 and 16%, while the composites with a PP content of 8 and 24% had the highest oxygen consumption. Figure 3b shows the relationship between the number of O₂ and time with PP contents of 24–40%. Among the five composites, the rapid oxygen consumption process in the first stage is 0–50 ps, which is 25 ps later than those with a PP content of 4–20%. In the first stage, the composite with 28% PP content had the fastest oxygen consumption rate, followed by that with 24% PP. The composite with 36% PP content had the slowest oxygen consumption rate. During the first phase of rapid combustion, the total oxygen consumption in the 24–40% PP composite was nearly the same. The average oxygen consumption in the five systems within 50 ps was 48 O₂. After 50 ps, the system entered the slow oxygen consumption stage. The system with 28% PP content had the most stable change of molecular oxygen number with time and the lowest oxygen consumption during this stage. The composite with 40% PP content had the highest oxygen consumption rate. In the slow oxygen consumption stage of the second stage, compared with the composite with a PP content of 25–40% and with a PP content of 4–20%, the number of O₂ is significantly different, the range of fluctuation is also more extensive, and the oxygen consumption is unstable. When the PP content in the composite is between 44 and 60% (Figure 3c), during the rapid oxygen consumption in the first stage, the oxygen consumption rate of the five systems is the same, and the average oxygen consumption is similar. The number of O₂ transformed is about 40. Among them, the composite with 44% PP content has the highest oxygen consumption and the fastest oxygen consumption rate.

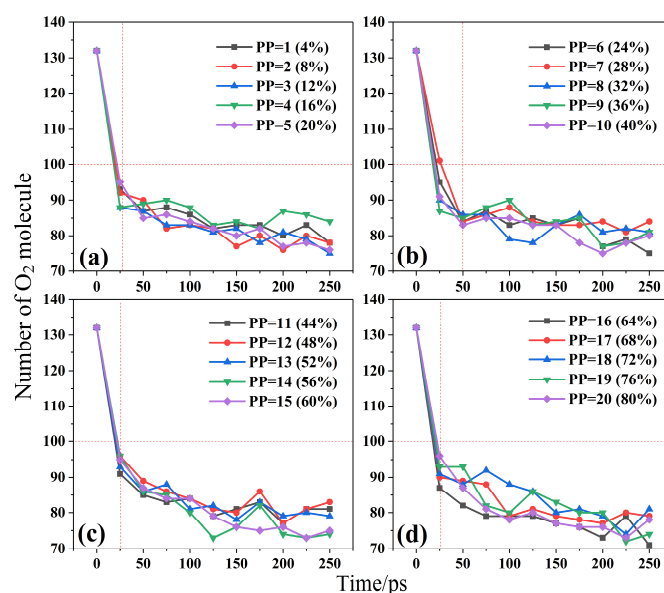


Figure 3. Oxygen consumption for PP/ZS composites combustion at temperature = 1000 K when PP = 1–5 (a); when PP = 6–10 (b); when PP = 11–15 (c); when PP = 16–20 (d).

In comparison, the system with 48% PP content has the slowest oxygen consumption rate and the lowest oxygen consumption. Among them, the composite with 44% PP content had the highest oxygen consumption and the fastest oxygen consumption rate, while the system with 48% PP content had the slowest oxygen consumption rate and the lowest oxygen consumption rate. After 25 ps, the five composites began to carry out the second stage of slow oxygen consumption. Within 25–100 ps, the number of O₂ in the

five systems changed steadily, and the slow oxygen consumption was stable. After 100 ps, the number of O₂ fluctuated wildly. Among them, the composite with 60% PP content gradually accelerated the oxygen consumption rate and increased oxygen consumption, becoming the system with the highest total oxygen consumption. The composite with 44% PP content also had stable oxygen consumption, but its total oxygen consumption was the lowest and reached a steady state of oxygen consumption after 125 ps. Figure 3d shows the number of O₂ in the system with 64–80% PP. Of the five systems, 0–25 ps is the first stage of rapid oxygen consumption. In this stage, oxygen consumption differs significantly. The composite with 80% PP consumed the least oxygen, and the number of O₂ transformed was 37. The composite with 64% PP consumes the most oxygen, and the number of O₂ converted is 46. After 25 ps, there was a significant difference in the number of O₂ among the five systems. The total oxygen consumption of the composite with 64% PP was the highest, and the number of O₂ changed steadily with time. The O₂ in the composite with 72% PP tended to increase within 50–75 ps. This composite has the lowest total oxygen consumption. The change of oxygen in the composite with 80% PP content was stable, and the total oxygen consumption was similar to that with 64% PP content.

The higher the PP content in the composite, the higher the oxygen consumption. Moreover, the higher the content of PP, the greater the difference in the number of O₂ in the slow oxygen consumption stage and the more pronounced the fluctuation. The rapid oxygen consumption stage of the system is 25–50 ps. Currently, the system with the fastest oxygen consumption rate is composite with 36 and 64% PP, and those for the slowest oxygen consumption rate are PP = 28/80/56/20%. The systems with the most significant difference in oxygen consumption rate are systems (b) and (d). The system with the most stable oxygen consumption rate in the slow oxygen consumption stage is PP = 4/20% composites. The difference in oxygen consumption is significant, and the composites with considerable fluctuation over time are PP = 44–80%.

2.3. Effect of Temperature and Content on Combustion Products

To reveal the influence of different temperatures and PP content on the combustion phenomenon and cracking mechanism, evolutions for carbon-containing intermediates and the products in 20 PP/ZS composites were analyzed. The pyrolysis product distribution of ZS/PP with different formulations at medium and high temperatures is shown in Figures 4 and 5, respectively. As the PP in the composite does not crack at low temperatures, almost no intermediates containing carbon numbers 1–30 and other combustion products were generated. This study did not elaborate on the product formation at 1000 K. Figures 4 and 5 analyze the evolution of intermediates in 20 kinds of PP/ZS composites and intuitively reflect the decomposition of the polymer.

Figure 4 shows the time variation of C1–C30 fragment number for 20 PP composites at 1500 K. When the PP content is 28/36–56/68–80%, the combustion reaction will generate C1–C4 fragments (Figure 4a,b for variation trend of the quantity of C1–C4 intermediates). It can be seen from Figure 4a that the composite with 28/36% PP content generates C1–C4 intermediates after 200 ps. When the PP content was 40%, C1–C4 fragments appeared after 150 ps, with a maximum of C1–C4 fragments. It can be seen from Figure 4b that when the content of PP is greater than 10, the earliest occurrence of C1–C4 intermediates in the composite is PP = 80%, and the composite with PP = 52% generates C1–C4 after 225 ps. When the PP content is 56/72%, the number of C1–C4 intermediates has a maximum value of three. When the PP content is 56%, the amount of C1–C4 in the system has a downward trend within 225–250 ps. Figure 4c,d shows the changes in intermediate fragments containing C5–C16 carbon. It can be seen from the statistics that C5–C16 intermediates will appear in the combustion process of the PP/ZS composites.

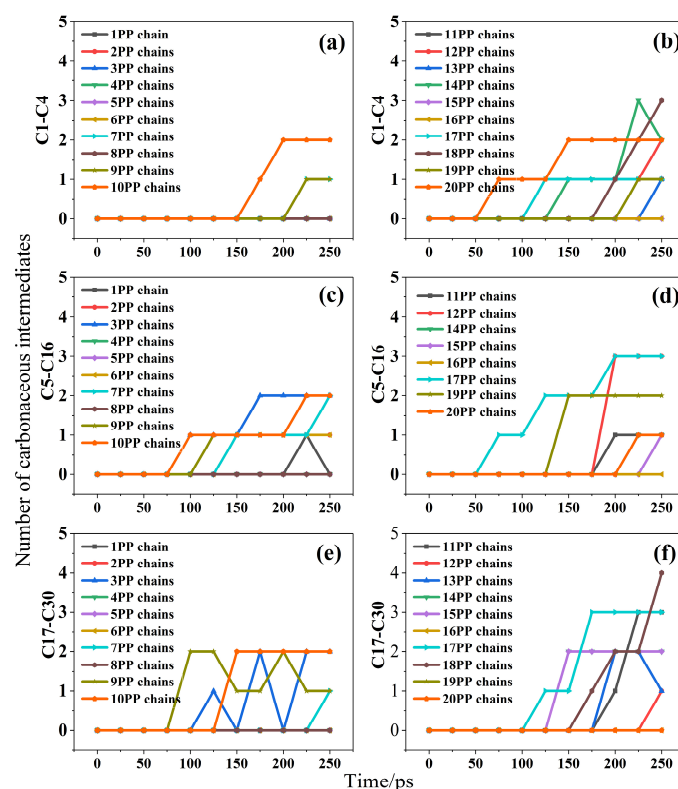


Figure 4. Changes in various carbon-containing fragments for 20 PP/ZS composites at temperature 1500 K. (a) C1–C4 in 1–10 PP; (b) C1–C4 in 11–20 PP; (c) C5–C16 in 1–10 PP; (d) C5–C16 in 11–20 PP; (e) C17–C30 in 1–10 PP; (f) C17–C30 in 11–20 PP.

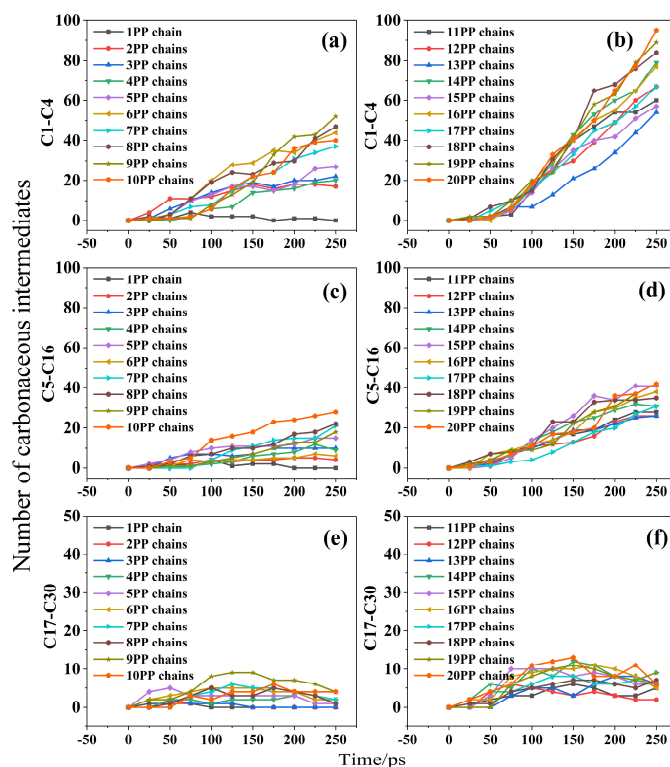


Figure 5. Changes in various carbon-containing fragments for 20 PP/ZS composites at temperature 2000 K. (a) C1–C4 in 1–10 PP; (b) C1–C4 in 11–20 PP; (c) C5–C16 in 1–10 PP; (d) C5–C16 in 11–20 PP; (e) C17–C30 in 1–10 PP; (f) C17–C30 in 11–20 PP.

From Figure 4d, C5–C16 fragments appear at the earliest in the combustion process of the PP = 68% composite, the time of the intermediate's emergence is 50 ps, and the maximum number of cracked fragments is reached at 200 ps. The second is the PP = 36 and 40% composites. The composite with PP = 60% has the latest emergence time of C5–C16 intermediates, followed by the composite with PP = 5%. When the content of PP was 12–76%, the number of C5–C16 fragments was the highest in the system. The number of systems producing C5–C16 is more in the system than that of C1–C4 intermediates.

Moreover, the generation time of C5–C16 is earlier than that of C1–C4, and the number of generated fragments is greater. Figure 4e,f shows the changes in intermediates containing C17–C30. It can be seen that when the content of PP is 4/8/16–24/32/64/76/80%, the composite will not crack into C17–C30 intermediates and the occurrence time of such intermediaries is 70 ps. Figure 4e shows that the generation time of C17–C30 mediators is the earliest in the PP = 36% system, followed by the PP = 12%/68% system. According to Figure 4f, the C17–C30 intermediate of the PP = 18 system appeared after 150 ps, reached the maximum value at 250 ps, and cleaved into four C17–C30 fragments, followed by PP = 68% system, with a maximum of three cleaved fragments.

By comparing Figure 4a–f, the earliest fragments in the system at 1500 K are C5–C16, C1–C4 has the fewest intermediates, and C17–C30 has the most significant mediators. With PP = 80%, C1–C4 intermediate appears early in the combustion process and has many fragments. C5–C16 intermediates occur earliest when PP = 68%. The C5–C16 intermediaries have the highest concentration in this system. When the PP content is 36%, C17–C30 appears first in the system, and the most significant number of these intermediaries is in the PP = 72% composite.

Figure 5a,b shows the evolutions of C1–C4 intermediates with time. The number of C1–C4 intermediates increases continuously with the combustion reaction at 2000 K. With the increase of the PP contents in the composites, C1–C4 intermediaries also increased gradually. It can be seen from Figure 5a that the number of C1–C4 intermediates is low in the composite with PP = 4%, and the maximum number of carbo-containing intermediaries is reached at 75 ps with four fragments. At 2000 K, the number of C1–C4 intermediates produced by the combustion process is about 0–50 for composites with 4–40% PP. Figure 5b shows that the system with the most significant number of C1–C4 mediators is the PP = 80% composite, which reaches 94 fragments by 250 ps. For the content of 44–80% PP system, the number of C1–C4 intermediates produced by the combustion process ranges from 50 to 100. Figure 5c,d shows the changes in C5–C16 intermediaries over time. Compared with that of C1–C4 fragments, the amount of C5–C16 generated was less affected by PP contents. According to Figure 5c, when there is 4–40% PP in the composites, the number of C5–C16 intermediates produced in the combustion process is about 0–20. According to Figure 5d, the highest number of C5–C16 arbitrators was generated at the end of the reaction for composite with PP = 80%. When the content of PP was 44–80%, the number of C5–C16 intermediaries ranged from 20 to 50. Figure 5e,f shows the variation of C17–C30 intermediates produced by 20 PP/ZS composites in the combustion with time. It can be seen that the number of C17–C30 fragments increases continuously within 0–150 ps, and the number of C17–C30 chips decreases within 150–250 ps. Compared with C1–C16 intermediates, the number of C17–C30 arbitrators was the least. They are also less affected by PP contents in the composites. When the PP content is 4–80%, the number of C17–C30 intermediates generated by combustion is between 0–15.

Figure 6 shows the evolutions of H₂O molecules with time in the combustion for 20 PP/ZS composites at different temperatures. When the temperature exceeds 1000 K, water molecules can be formed. Moreover, the number of water molecules is also increasing with the increase of PP content in the composites. The time of water molecules formed in the system is before 100 ps, and the occurrence time is independent of PP contents in composites. When the PP content is 4–16%, the number of water molecules generated by combustion is less than 10. When the PP is 20–52%, H₂O molecules are fewer than 20 in combustion.

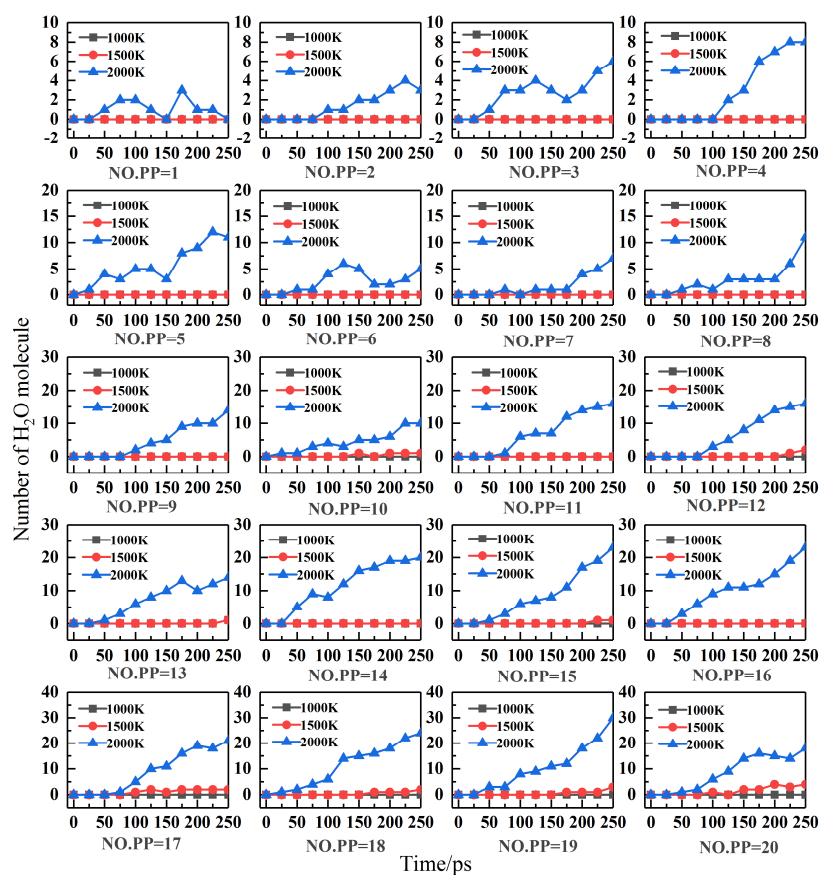


Figure 6. Changes in H₂O molecule number for 20 PP/ZS composites at different combustion temperatures.

The number of H₂O generated during combustion is less than 30 when the PP concentration in composites is 56–80%. When the PP content is more significant than 40% at 1500 K, H₂O molecule formation is possible. When PP content is 4–16%, the average H₂O generated increases by two for each additional PP cluster at 2000 K. The first system to create H₂O molecules was PP = 4 and 12%. The content of H₂O in the system showed a trend of increasing first and then decreasing. When PP = 8 and 16%, the number of H₂O generated showed an increasing trend in combustion. When PP = 20 and 24% in the composite, the H₂O produced increased first and then decreased in combustion. When the PP content in composites is greater than 24%, the number of H₂O created at 2000 K only exhibits an upward trend until 250 ps. The most significant amount of H₂O produced in combustion occurs at 2000 K and 250 ps when PP = 76% in the composite. At 1500 K, when the PP content was 40% in the composite, H₂O appeared for the first time in the combustion process, reaching the maximum value after 150 ps. The time distribution of its creation of H₂O is most significant when PP = 68%. When the PP is 80% in the composite, H₂O at 1500 K is the largest, with a maximum of four at 200 ps.

3. Models and Simulation Methods

3.1. ReaxFF Force Field

In order to make the content of the training set describes the C–H–O–Sn–Zn system more comprehensively, we select samples with different types and sizes as research training sets for the force field. The models of training sets have four groups. One is tin-based compounds, including SnO, Sn₅O₆, SnO₂, SnC, SnH₄, Sn(CO₂)₂, and Sn₃(HO₂)₂. The other is zinc-based compounds, including ZnH, ZnH₆, ZnC₃, ZnO, ZnO₂, Zn(HO)₂, ZnCO₃, and ZnH₄(CO₃)₂. The third is the tin–zinc structure, which includes three ZnSnO₃ unit cells (with space groups R3c, R $\bar{3}$, and Pnma, see Figure 7), Zn₂SnO₄, and ZnSn₂O₅. The last

is composed of C/H/O elements, which are relatively mature in previous ReaxFF MD simulations. Because the flame retardant effect of ZS bulk will be studied in this paper, the ZS cluster structures with different sizes are considered, and their energy calculation is added to the training sets [40].

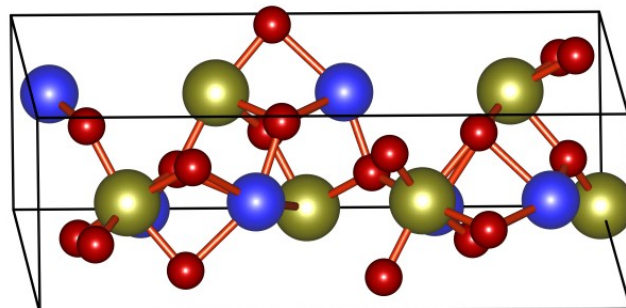


Figure 7. Unit structure of bulk ZS.

In order to build a more comprehensive and representative training set, the structural element should include as many chemical bonds, dihedral angles, and transition states as possible (see Figure S2). The structural state of the combustion system should also be considered, and attention should be paid to hydrogen bonding [41–44]. The ZnSnO_3 crystal with different space groups and other cell structures come from Materials Project, and some molecular structures are constructed by the Gauss View code. Here, we directly import the previously reported C/H/O parameters [41] for combustion reactions into the training set to be fitted and modify the needed parameters about bond energy, twist angle, dihedral angle, and other properties containing Zn and Sn atoms.

When the reasonable model of the training set is determined, these molecular structures are calculated by single point energy calculation, geometric optimization, and PES scanning, and then the force field parameters are fitted from the calculated results of these training sets [40,45,46]. These calculations are based on the first principles of the density functional theory (DFT) framework. DFT calculations use the B3LYP method and mixed basis sets (C/H/O element of 6-31G* and Zn/Sn of SDD pseudo-potential) [47–49]. Molecular structure DFT calculations were performed using the Gaussian16 [47]. The crystal structure with periodic boundary conditions is calculated using the Band module of the AMS code [40]. The findings are adapted to the new training set using the AMS and its suggested standard processes and methodologies. By optimizing the balanced training sets, the weight distribution is moderately changed to guarantee that the weight is increasingly skewed towards the combustion conditions of the PP structure (the process is shown in Figure 8).

The developed ReaxFF parameters are verified by the comparisons of DFT and ReaxFF calculations. The selection of verification sets includes the characteristic reaction in the combustion process of the target system, the formation process of the leading transition state, the metal elements, and the differential characteristics of the catalyst [50,51]. In this study, we construct the verification sets through the preliminary ReaxFF calculations of oxygen-rich ZS systems and the previous experimental reports [21]. It mainly includes metal elements bound by different carbon groups, metal oxides, metal-bound oxygen atoms, and the dissociation process of ZS. In the DFT and ReaxFF calculations, the scanning range and the bond length or angle are limited to the range below or above the equilibrium value, and the dissociation curve is constructed from the scanning results [52].

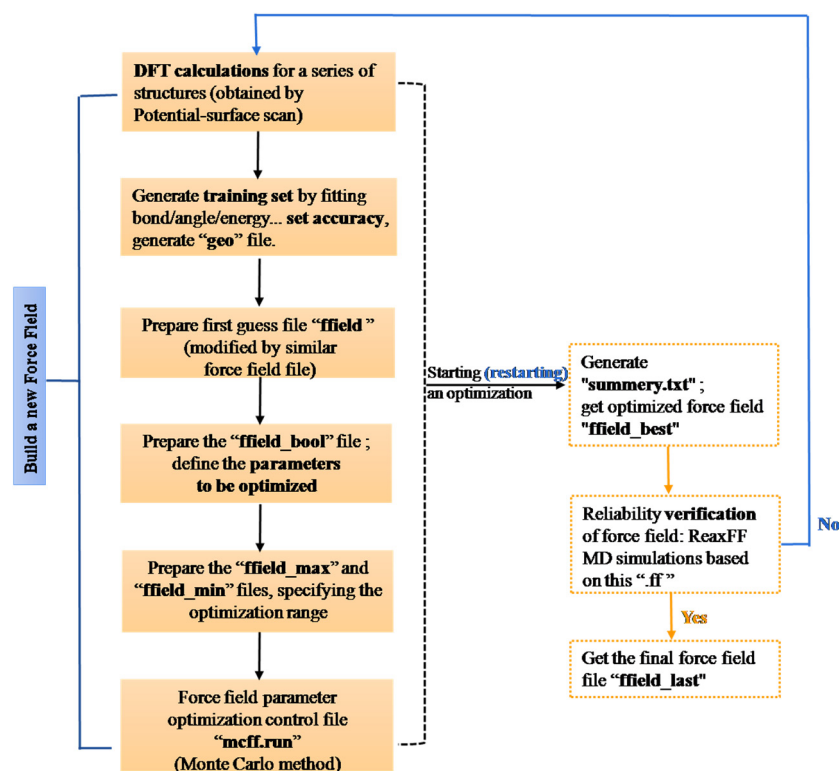


Figure 8. The process of building a new force field.

3.2. Details of ReaxFF MD Simulations

In ReaxFF MD simulations, the force field can dynamically optimize atomic charge using the electronegativity balance method [53] and the covalent form and bond order principle to simulate potential chemical reactions. They are associated with thermodynamic and kinetic properties on a microscopic scale [54,55]. The instantaneous bond order from a distance between atoms can be calculated by:

$$BO'_{ij} = \exp \left[p_{bo,1} \cdot \left(\frac{r_{ij}}{r_0} \right)^{p_{bo,2}} \right] + \exp \left[p_{bo,3} \cdot \left(\frac{r_{ij}^\pi}{r_0} \right)^{p_{bo,4}} \right] + \exp \left[p_{bo,5} \cdot \left(\frac{r_{ij}^{\pi\pi}}{r_0} \right)^{p_{bo,6}} \right] \quad (1)$$

The system energy of the force field consists of the energy of each part that can be obtained by:

$$E_{\text{system}} = E_{\text{Bond}} + E_{\text{over}} + E_{\text{under}} + E_{\text{lp}} + E_{\text{val}} + E_{\text{tor}} + E_{\text{vdWaals}} + E_{\text{Coulomb}} \quad (2)$$

The energy of the system in ReaxFF comes from the energy contribution items of different parts, including bond energies, valence angle, lone pair, conjugation, and torsion angle terms [56]. E_{system} is the system's potential energy, which is divided into reaction potential energy and non-reaction potential energy. The reaction potential energy accurately simulates the reaction between particles through the binding and dissociation between particles. The non-reaction potential energy affects the reaction's transition state and barrier energy. E_{Bond} is the bonding energy, which expresses the bond energy caused by the distance between atoms by calculating the bond order. To solve the problem of over-coordinated and under-coordinated atoms, E_{over} and E_{under} correct the system energy. The modified bond order BO'_{ij} is used in E_{over} to replace the unmodified bond order, thus ensuring that the under-corrected system will soon disappear to zero. Only when there is a π bond between the under-coordinated atom and its neighboring atoms is E_{under} 's correction of the system's potential energy meaningful. E_{val} is the energy of the valence angle term. The bond-order-dependent form is used to calculate the different energy

between the valence angle and its equilibrium value and to ensure that the valence angle contribution value returns to zero smoothly during the ion dissociation process [38]. Like the bonding value, the valence angle term also needs to discuss the over-coordination and under-coordination of the valence angle ability of the central atom. E_{tor} is the torsion angle energy. When a bond in the torsion angle breaks, its valence angle is close to π , and its torsion energy disappears smoothly. E_{vdWaals} is van der Waals energy and E_{Coulomb} is Coulomb energy. Due to the mutual attraction between particles due to dispersion and the fact that a repulsive force also exists in a short distance between particles, all atomic pairs should contain van der Waals force and Coulomb force to express the energy change in bond dissociation more completely.

The combustion reactions in mixed samples of PP and ZS at different temperatures were simulated using the ReaxFF MD method. In this study, the combustion process was simulated based on the PP molecular aggregation model, and the effects of different formula ratios and temperatures on the combustion mechanism of plastics were observed. In order to obtain a balanced and uniform reactant and prevent the unreliable results of molecular dynamics simulation due to the unreasonable initial structure, the relaxation domains of 20 composites were carried out before the formal ReaxFF molecular dynamics simulation. To ensure that the system does not react in the relaxation region and maintain the state of the reactants, we chose to carry out a 50,000-step relaxation process at 450 K. The combustion reaction of the different ZS/PP composites was simulated with the effects of temperature. For this, the combustion temperature is set to 1000, 1500, and 2000 K, respectively. The choice of experimental temperature and simulated temperature is not comparable. The simulated temperature here is much higher than the real one. This is because artificially increasing the simulation temperature is a widely used simulation strategy in ReaxFF MD to explore organic molecular systems' pyrolysis and oxidation reaction mechanisms [57]. This is a typical setting in the ReaxFF simulation of pyrolysis/combustion and other thermochemical reactions and has been widely accepted [58].

The time step in MD is set to 0.25 fs with a total of 1,000,000 steps, that is, the total duration of 250 ps. The setting of the above combustion reaction parameters is consistent with the reported parameters used to study the reaction mechanism of thermochemical processes such as pyrolysis and combustion by the ReaxFF MD method [51]. All the ReaxFF MD calculations and analyses are done on the AMS platform.

3.3. Theoretical Models

ZS is a kind of commercial inorganic flame retardant, which belongs to the ordinary flameless flame retardant. Unlike reactive additives, normal additives do not chemically bond to the polymer; they are incorporated into the polymer during the polymerization process or during the melt mixing of thermoplastic materials. ZS generally acts as a flame retardant aid, providing thermal insulation for polymers by forming a carbon protective layer, and thus plays a role in the condensed phase. Due to the principle of chemical flame retardant of ZS, we did not consider the influence of interface reaction and PP polymerization degree. The model building details are as follows.

A PP model with a molecular formula of $\text{C}_{45}\text{H}_{92}$ is constructed by Gaussview in this work. This PP structure and buck ZS crystal are optimized using density functional theory calculations with B3LYP combined cc-pVDZ or DZP basis sets. A $42 \times 42 \times 100 \text{ \AA}^3$ box with a periodic boundary condition is built with $8 \times 8 \times 6$ ZS unit cells at the upper and lower sides (Figure 9a). Then this box is filled with 1–20 PP aggregation models in the central part in order to construct 20 different ZS/PP composite models with various contents. In one periodic box, we put in a sufficient number of oxygen molecules to oxidize all PP molecules in each composite system. The flame retardant property was further compared by comparing oxygen consumption. Finally, these 20 periodic boxes were randomly filled with 132 O_2 molecules in the free space (Figures 9 and S1 in Supplementary Material). In these 20 models of ZS/PP composites to perform the ReaxFF MD simulation in the next step, the PP content varies from 4% to 80%.

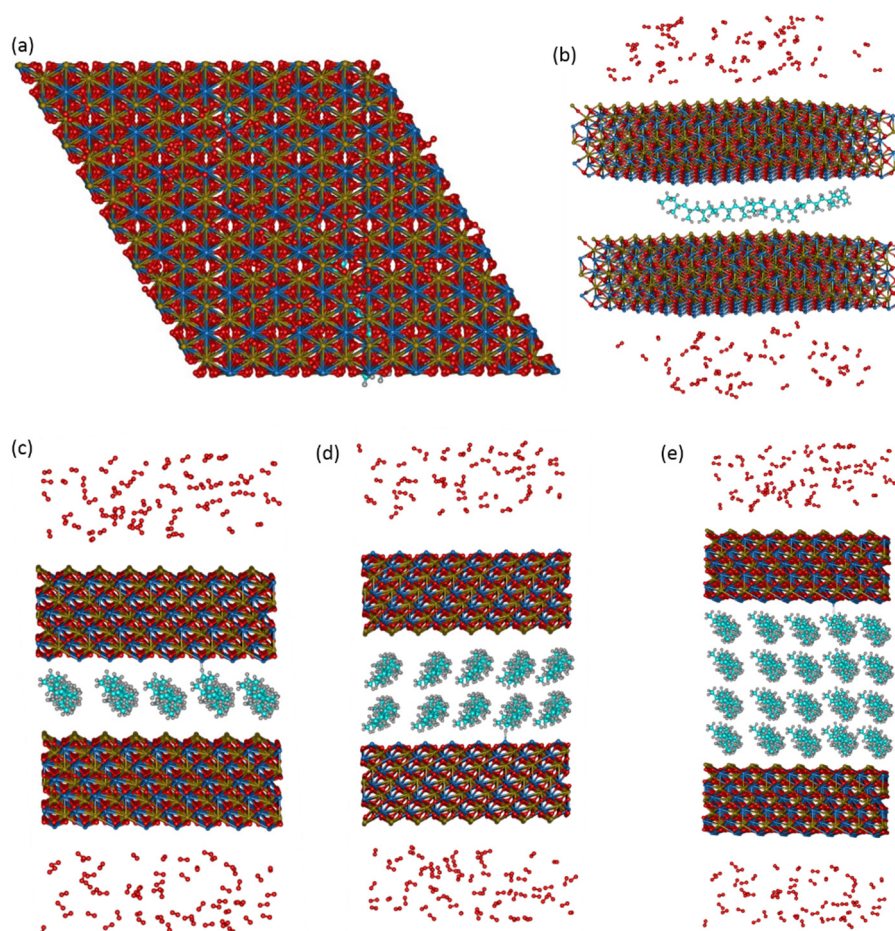


Figure 9. Models of ZS/PP composites with different ratios for combustions. (a) Top view; (b) side view of PP = 1 with content 4%; (c) PP = 5 with content 20%; (d) PP = 10 with content 40%; (e) PP = 20 with content 80%.

4. Conclusions

In this work, the flame retardant mechanism of ZS/PP composites has been studied using ReaxFF MD simulations. The main conclusions are as follows:

- (1) A ReaxFF force field including Sn/Zn/C/H/O elements was developed for ZS/PP combustion. By determining the essential chemical information in the flame-retardant system, various ground state structures, such as ZS crystals and clusters, were selected to conduct DFT calculations with selected training sets. The accuracy of obtained force field parameters was verified. By comparing DFT and ReaxFF calculations, the dissociation distance error was within 0.15 Å, while the bond angle error was within 2.5°. The results from QM and ReaxFF concur well for each energy proofreading circumstance.
- (2) ReaxFF MD simulations were conducted for the combustion reactions of 20 different PP/ZS composites at different temperatures. The results demonstrate that temperature limits the degree of combustion by influencing the molecular oxygen consumption of PP cracking, suggesting the flame retardant feature of ZS. The higher the combustion temperature, the slower the oxygen consumption rate of PP/ZS composites and the lower the total oxygen consumption. When the PP component of composites exceeds 56%, oxygen consumption increases. The rapid oxygen consumption stage of combustion is 25–50 ps, followed by the second slow oxygen consumption stage 50 ps later. The higher the PP percentage in composites, the more oxygen is consumed at the same temperature.
- (3) No intermediates smaller than C30 were detected in PP/ZS combustions at 1000 K. The earliest intermediary is C5–C16, while the latest is C1–C4. C17–C30 is the intermediate

for PP/ZS composite combustions at 1500 K. The combustion process produces C1–C30 mediators at a temperature of 2000 K. The amount of the C1–C4 mediator was the highest, and C17–C30 was the lowest. The higher the PP percentage, the more C1–C16 fragments are formed during combustion. According to the ReaxFF MD simulations, molecular H₂O can form at reaction temperatures beyond 1000 K. The number of H₂O in PP/ZS composites increases with PP concentration.

Supplementary Materials: The following supporting information can be downloaded at: <https://www.mdpi.com/article/10.3390/inorganics11060233/s1>, Figure S1: Models of 20 different ZS/PP composites with various ratios for combustions. Figure S2: Structures of partial training set. (a) Scanning of different bonds, angles, and transition states; (b) Scanning of ZS crystals with different space groups.

Author Contributions: Conceptualization, C.G. and H.B.; methodology, C.G. and H.B.; validation, M.Z., J.L., C.G. and S.Y.; formal analysis, C.G. and L.M.; investigation, H.Z., Y.W., Y.Z. and R.F.; resources, J.L., Y.Y. and Z.F.; data curation, J.L., C.G., S.Y. and R.F.; writing—original draft, J.L. and C.G.; writing—review and editing, C.G. and H.B.; visualization, H.Z.; supervision, H.B.; project administration, J.L. and H.B.; funding acquisition, J.L., Y.Y. and Z.F. All authors have read and agreed to the published version of the manuscript.

Funding: This research was funded by Yunnan Province Major Science and Technology Special Program (No.202002AB080001-2), Yunnan Province Major Science and Technology Special Program (No.202102AB080002), and Yunnan Province “Ten Thousand Talents Plan” Industrial Technology Leading Talent Program (No. YNWR-CYJS-2017-056).

Data Availability Statement: Not applicable.

Conflicts of Interest: The authors declare no conflict of interest.

References

1. Rad, E.R.; Vahabi, H.; de Anda, A.R.; Saeb, M.R.; Thomas, S. Bio-epoxy resins with inherent flame retardancy. *Prog. Org. Coat.* **2019**, *135*, 608–612. [[CrossRef](#)]
2. Seidi, F.; Movahedifar, E.; Naderi, G.; Akbari, V.; Ducos, F.; Shamsi, R.; Vahabi, H.; Saeb, M.R. Flame retardant polypropylenes: A review. *Polymers* **2020**, *12*, 1701. [[CrossRef](#)] [[PubMed](#)]
3. Vahabi, H.; Jouyandeh, M.; Cochez, M.; Khalili, R.; Vagner, C.; Ferriol, M.; Movahedifar, E.; Ramezanzadeh, B.; Rostami, M.; Ranjbar, Z. Short-lasting fire in partially and completely cured epoxy coatings containing expandable graphite and halloysite nanotube additives. *Prog. Org. Coat.* **2018**, *123*, 160–167. [[CrossRef](#)]
4. Zhang, Z.X.; Zhang, J.; Lu, B.-X.; Xin, Z.X.; Kang, C.K.; Kim, J.K. Effect of flame retardants on mechanical properties, flammability and foamability of PP/wood-fiber composites. *Compos. Part B Eng.* **2012**, *43*, 150–158. [[CrossRef](#)]
5. Renner, G.; Nellessen, A.; Schwiers, A.; Wenzel, M.; Schmidt, T.C.; Schram, J. Data preprocessing & evaluation used in the microplastics identification process: A critical review & practical guide. *TrAC Trends Anal. Chem.* **2019**, *111*, 229–238.
6. Maddah, H.A. Polypropylene as a promising plastic: A review. *Am. J. Polym. Sci.* **2016**, *6*, 1–11.
7. Shen, R.; Quan, Y.; Zhang, Z.; Ma, R.; Wang, Q. Metal-Organic Framework as an Efficient Synergist for Intumescent Flame Retardants against Highly Flammable Polypropylene. *Ind. Eng. Chem. Res.* **2022**, *61*, 7292–7302. [[CrossRef](#)]
8. Pan, Y.; Luo, Z.; Wang, B. Synergistic flame retardant effect of piperazine salt and ammonium polyphosphate as intumescent flame retardant system for polypropylene. *J. Appl. Polym. Sci.* **2021**, *138*, 49813. [[CrossRef](#)]
9. Zhang, Q.; Zhan, J.; Zhou, K.; Lu, H.; Zeng, W.; Stec, A.A.; Hull, T.R.; Hu, Y.; Gui, Z. The influence of carbon nanotubes on the combustion toxicity of PP/intumescent flame retardant composites. *Polym. Degrad. Stab.* **2015**, *115*, 38–44. [[CrossRef](#)]
10. Zhang, S.; Horrocks, A.R. A review of flame retardant polypropylene fibres. *Prog. Polym. Sci.* **2003**, *28*, 1517–1538. [[CrossRef](#)]
11. Vahabi, H.; Paran, S.M.R.; Shabani, M.; Dumazert, L.; Sonnier, R.; Movahedifar, E.; Zarrintaj, P.; Saeb, M.R. Triple-faced polypropylene: Fire retardant, thermally stable, and antioxidative. *J. Vinyl Addit. Technol.* **2019**, *25*, 366–376. [[CrossRef](#)]
12. Li, B.; Xu, M. Effect of a novel charring-foaming agent on flame retardancy and thermal degradation of intumescent flame retardant polypropylene. *Polym. Degrad. Stab.* **2006**, *91*, 1380–1386. [[CrossRef](#)]
13. Vahabi, H.; Kandola, B.K.; Saeb, M.R. Flame retardancy index for thermoplastic composites. *Polymers* **2019**, *11*, 407. [[CrossRef](#)] [[PubMed](#)]
14. Vahabi, H.; Dumazert, L.; Khalili, R.; Saeb, M.R.; Cuesta, J.-M.L. Flame retardant PP/PA6 blends: A recipe for recycled wastes. *Flame Retard. Therm. Stab. Mater.* **2019**, *2*, 1–8. [[CrossRef](#)]
15. Pani, B.; Sirohi, S.; Singh, D. Studies on the effects of various flame retardants on polypropylene. *Am. J. Polym. Sci.* **2013**, *3*, 63–69.
16. Li, Y.-M.; Hu, S.-L.; Wang, D.-Y. Polymer-based ceramifiable composites for flame retardant applications: A review. *Compos. Commun.* **2020**, *21*, 100405. [[CrossRef](#)]

17. Thien, N.D.; Quynh, L.M.; Van Vu, L.; Long, N.N. Phase transformation and photoluminescence of undoped and Eu^{3+} -doped zinc stannate (Zn_2SnO_4) nanocrystals synthesized by hydrothermal method. *J. Mater. Sci. Mater. Electron.* **2019**, *30*, 1813–1820. [[CrossRef](#)]
18. Keles, E.; Yildirim, M.; Öztürk, T.; Yildirim, O.A. Hydrothermally synthesized UV light active zinc stannate:tin oxide (ZTO:SnO₂) nanocomposite photocatalysts for photocatalytic applications. *Mater. Sci. Semicond. Process.* **2020**, *110*, 104959. [[CrossRef](#)]
19. Levchik, S.V.; Weil, E.D. Combustion and fire retardancy of aliphatic nylons. *Polymer International.* **2000**, *49*, 1033–1073. [[CrossRef](#)]
20. Horrocks, A.; Smart, G.; Price, D.; Kandola, B. Zinc stannates as alternative synergists in selected flame retardant systems. *J. Fire Sci.* **2009**, *27*, 495–521. [[CrossRef](#)]
21. Zhong, F.; Chen, C.; Yang, X.; Zhou, J.; Zheng, W.; Huang, H.; Wang, P.; Li, W. Self-assembly of zinc hydroxystannate on polyethyleneimine supported boron nitride to improve the flame protection properties of waterborne epoxy coatings. *Colloids Surf. A Physicochem. Eng. Asp.* **2022**, *650*, 129557. [[CrossRef](#)]
22. Horrocks, A.; Smart, G.; Kandola, B.; Price, D. Zinc stannate interactions with flame retardants in polyamides; Part 2: Potential synergies with non-halogen-containing flame retardants in polyamide 6 (PA6). *Polym. Degrad. Stab.* **2012**, *97*, 645–652. [[CrossRef](#)]
23. Wu, W.; Qu, H.; Li, Z.; Yuan, H. Thermal behavior and flame retardancy of flexible poly (vinyl chloride) treated with zinc hydroxystannate and zinc stannate. *J. Vinyl Addit. Technol.* **2008**, *14*, 10–15. [[CrossRef](#)]
24. Morgan, A.B.; Gilman, J.W. An overview of flame retardancy of polymeric materials: Application, technology, and future directions. *Fire Mater.* **2013**, *37*, 259–279. [[CrossRef](#)]
25. Hansen, N.; Cool, T.A.; Westmoreland, P.R.; Kohse-Höinghaus, K. Recent contributions of flame-sampling molecular-beam mass spectrometry to a fundamental understanding of combustion chemistry. *Prog. Energy Combust. Sci.* **2009**, *35*, 168–191. [[CrossRef](#)]
26. Laoutid, F.; Bonnaud, L.; Alexandre, M.; Lopez-Cuesta, J.M.; Dubois, P. New prospects in flame retardant polymer materials: From fundamentals to nanocomposites. *Mater. Sci. Eng. R Rep.* **2009**, *63*, 100–125. [[CrossRef](#)]
27. Altarawneh, M.; Saeed, A.; Al-Harashsheh, M.; Dlugogorski, B.Z. Thermal decomposition of brominated flame retardants (BFRs): Products and mechanisms. *Prog. Energy Combust. Sci.* **2019**, *70*, 212–259. [[CrossRef](#)]
28. Sai, T.; Ran, S.; Guo, Z.; Song, P.; Fang, Z. Recent advances in fire-retardant carbon-based polymeric nanocomposites through fighting free radicals. *SusMat* **2022**, *2*, 411–434. [[CrossRef](#)]
29. Liu, S.; Wei, L.; Zhou, Q.; Yang, T.; Li, S.; Zhou, Q. Simulation strategies for ReaxFF molecular dynamics in coal pyrolysis applications: A review. *J. Anal. Appl. Pyrolysis* **2023**, *170*, 105882. [[CrossRef](#)]
30. Guo, S.T.; Liu, J.; Qian, W.; Zhu, W.H.; Zhang, C.Y. A review of quantum chemical methods for treating energetic molecules. *Energetic Mater. Front.* **2021**, *2*, 239–316. [[CrossRef](#)]
31. Han, Y.; Jiang, D.; Zhang, J.; Li, W.; Gan, Z.; Gu, J. Development, applications and challenges of ReaxFF reactive force field in molecular simulations. *Front. Chem. Sci. Eng.* **2016**, *10*, 16–38. [[CrossRef](#)]
32. Yuen, A.C.Y.; Chen, T.B.Y.; Li, A.; De Cachinho Cordeiro, I.M.; Liu, L.; Liu, H.; Lo, A.L.P.; Chan, Q.N.; Yeoh, G.H. Evaluating the fire risk associated with cladding panels: An overview of fire incidents, policies, and future perspective in fire standards. *Fire Mater.* **2021**, *45*, 663–689. [[CrossRef](#)]
33. Yang, K.; Wu, R.; Shen, L.; Feng, Y.P.; Dai, Y.; Huang, B. Origin of d^0 magnetism in II-VI and III-V semiconductors by substitutional doping at anion site. *Phys. Rev. B* **2010**, *81*, 125211. [[CrossRef](#)]
34. Shetty, S.; Pal, S.; Kanhere, D.G.; Goursot, A. Structural, Electronic, and Bonding Properties of Zeolite Sn-Beta: A Periodic Density Functional Theory Study. *Chem. Eur. J.* **2006**, *12*, 518–523. [[CrossRef](#)] [[PubMed](#)]
35. Wong-Ng, W.; Luo, T.; Xie, W.; Tang, W.H.; Kaduk, J.A.; Huang, Q.; Yan, Y.; Chattopadhyay, S.; Tang, X.; Tritt, T. Phase diagram, crystal chemistry and thermoelectric properties of compounds in the Ca–Co–Zn–O system. *J. Solid State Chem.* **2011**, *184*, 2159–2166. [[CrossRef](#)]
36. Zhou, B.; Denning, M.S.; Jones, C.; Goicoechea, J.M. Reductive cleavage of Zn–C bonds by group 14 Zintl anions: Synthesis and characterization of $[\text{E}_9\text{ZnR}]^{3-}$ (E = Ge, Sn, Pb; R = Mes, iPr). *Dalton Trans.* **2009**, *9*, 1571–1578. [[CrossRef](#)] [[PubMed](#)]
37. Li, J.; Peng, C.; Li, J.; Wang, J.; Zhang, H. Insight into Sodium Storage Behaviors in Hard Carbon by ReaxFF Molecular Dynamics Simulation. *Energy Fuels* **2022**, *36*, 5937–5952. [[CrossRef](#)]
38. Krebs, B.; Henkel, G.; Dartmann, M. Structure of tetramethyltin, $\text{Sn}(\text{CH}_3)_4$. *Acta Crystallogr. Sect. C Cryst. Struct. Commun.* **1989**, *45*, 1010–1012. [[CrossRef](#)]
39. Wang, Q.; Yan, L.; Meng, L.; Zhang, J.; Li, H.; Geng, C.; Bai, H.; Guo, Q. Mechanism and process of chemical looping depolymerization of polyethylene based on iron-based oxygen carriers. *Acta Pet. Sin. (Pet. Process. Sect.)* **2023**, *39*, 358–367.
40. Chenoweth, K.; Van Duin, A.C.; Goddard, W.A. ReaxFF reactive force field for molecular dynamics simulations of hydrocarbon oxidation. *J. Phys. Chem. A* **2008**, *112*, 1040–1053. [[CrossRef](#)]
41. Boes, J.R.; Groenenboom, M.C.; Keith, J.A.; Kitchin, J.R. Neural network and ReaxFF comparison for Au properties. *Int. J. Quantum Chem.* **2016**, *116*, 979–987. [[CrossRef](#)]
42. Han, S.S.; Van Duin, A.C.; Goddard, W.A., III; Lee, H.M. Optimization and application of lithium parameters for the reactive force field, ReaxFF. *J. Phys. Chem. A* **2005**, *109*, 4575–4582. [[CrossRef](#)] [[PubMed](#)]
43. Cavallotti, C.; Moscatelli, D.; Masi, M.; Carrà, S. Accelerated decomposition of gas phase metal organic molecules determined by radical reactions. *J. Cryst. Growth* **2004**, *266*, 363–370. [[CrossRef](#)]
44. Abdulsattar, M.A.; Jabbar, R.H.; Abed, H.H. Transition state application to simulate CO gas sensor of pristine and Pt doped tin dioxide clusters. *J. Phys. Conf. Ser.* **2021**, *1963*, 012033. [[CrossRef](#)]

45. Senftle, T.P.; Meyer, R.J.; Janik, M.J.; Van Duin, A.C. Development of a ReaxFF potential for Pd/O and application to palladium oxide formation. *J. Chem. Phys.* **2013**, *139*, 044109. [[CrossRef](#)]
46. Rahaman, O.; Van Duin, A.C.; Goddard, W.A., III; Doren, D.J. Development of a ReaxFF reactive force field for glycine and application to solvent effect and tautomerization. *J. Phys. Chem. B* **2011**, *115*, 249–261. [[CrossRef](#)] [[PubMed](#)]
47. Chenoweth, K.; Van Duin, A.C.; Persson, P.; Cheng, M.-J.; Oxgaard, J.; Goddard, W.A., III. Development and application of a ReaxFF reactive force field for oxidative dehydrogenation on vanadium oxide catalysts. *J. Phys. Chem. C* **2008**, *112*, 14645–14654. [[CrossRef](#)]
48. Depew, D.D.; Wang, J.; Parmar, S.; Chambreau, S.; Bedrov, D.; van Duin, A.; Vaghjiani, G. *AIAA Propulsion and Energy 2019 Forum*; American Institute of Aeronautics and Astronautics: Reston, VA, USA, 2019.
49. Shchygol, G.; Yakovlev, A.; Trnka, T.; Van Duin, A.C.; Verstraelen, T. ReaxFF parameter optimization with Monte-Carlo and evolutionary algorithms: Guidelines and insights. *J. Chem. Theory Comput.* **2019**, *15*, 6799–6812. [[CrossRef](#)]
50. Nielson, K.D.; Van Duin, A.C.; Oxgaard, J.; Deng, W.-Q.; Goddard, W.A., III. Development of the ReaxFF reactive force field for describing transition metal catalyzed reactions, with application to the initial stages of the catalytic formation of carbon nanotubes. *J. Phys. Chem. A* **2005**, *109*, 493–499. [[CrossRef](#)] [[PubMed](#)]
51. Van Duin, A.C.; Bryantsev, V.S.; Diallo, M.S.; Goddard, W.A., III; Rahaman, O.; Doren, D.J.; Raymand, D.; Hermansson, K. Development and validation of a ReaxFF reactive force field for Cu cation/water interactions and copper metal/metal oxide/metal hydroxide condensed phases. *J. Phys. Chem. A* **2010**, *114*, 9507–9514. [[CrossRef](#)]
52. Huang, Y.; Wexler, A.S.; Bein, K.J.; Faller, R. Development of a ReaxFF Force Field for Aqueous Phosphoenolpyruvate as a Novel Biomimetic Carbon Capture Absorbent. *J. Phys. Chem. C* **2022**, *126*, 9284–9292. [[CrossRef](#)]
53. Zheng, M.; Li, X.; Guo, L. Algorithms of GPU-enabled reactive force field (ReaxFF) molecular dynamics. *J. Mol. Graph. Model.* **2013**, *41*, 1–11. [[CrossRef](#)] [[PubMed](#)]
54. Sengul, M.Y.; Song, Y.; Nayir, N.; Gao, Y.; Hung, Y.; Dasgupta, T.; van Duin, A.C. INDEEDopt: A deep learning-based ReaxFF parameterization framework. *Npj Comput. Mater.* **2021**, *7*, 1–9. [[CrossRef](#)]
55. Russo, M.F., Jr.; Van Duin, A.C. Atomistic-scale simulations of chemical reactions: Bridging from quantum chemistry to engineering. *Nucl. Instrum. Methods Phys. Res. Sect. B Beam Interact. Mater. At.* **2011**, *269*, 1549–1554. [[CrossRef](#)]
56. Van Duin, A.C.; Strachan, A.; Stewman, S.; Zhang, Q.; Xu, X.; Goddard, W.A., III. ReaxFF SiO reactive force field for silicon and silicon oxide systems. *J. Phys. Chem. A* **2003**, *107*, 3803–3811. [[CrossRef](#)]
57. Li, X.; Zheng, M.; Ren, C.; Guo, L. Reaxff molecular dynamics simulations of thermal reactivity of various fuels in pyrolysis and combustion. *Energy Fuels* **2021**, *35*, 11707–11739. [[CrossRef](#)]
58. Mueller, J.E.; van Duin, A.C.T.; Goddard, W.A., III. Application of the Reaxff reactive force field to reactive dynamics of hydrocarbon chemisorption and decomposition. *J. Phys. Chem. C* **2010**, *114*, 5675–5685. [[CrossRef](#)]

Disclaimer/Publisher’s Note: The statements, opinions and data contained in all publications are solely those of the individual author(s) and contributor(s) and not of MDPI and/or the editor(s). MDPI and/or the editor(s) disclaim responsibility for any injury to people or property resulting from any ideas, methods, instructions or products referred to in the content.